Inorganic Chemistry

Article

pubs.acs.org/IC

Probing the Electronic Structure and Chemical Bonding in Tricoordinate Uranyl Complexes $UO_2X_3^-$ (X = F, Cl, Br, I): Competition between Coulomb Repulsion and U−X Bonding

Jing Su,[†] Phuong Diem Dau,[‡] Yi-Heng Qiu,[†] Hong-Tao Liu,[‡] Chao-Fei Xu,[†] Dao-Ling Huang,[‡] Lai-Sheng Wang,*[,‡] and Jun Li*[,†]

[†]Department of Chemistry & Key Laboratory of Organic Optoelectronics and Molecular Engineering of Ministry of Education, Tsinghua University, Beijing 100084, China

[‡]Department of Chemistry, Brown University, Providence, Rhode Island 02912, United States

Supporting Information

ABSTRACT: While uranyl halide complexes $[UO_2(halogen)_n]^{2-n}$ (n = 1, 2, 4) are ubiquitous, the tricoordinate species have been relatively unknown until very recently. Here photoelectron spectroscopy and relativistic quantum chemistry are used to investigate the bonding and stability of a series of gaseous tricoordinate uranyl complexes, $UO_2X_3^-$ (X = F, Cl, Br, I). Isolated $UO_2X_3^-$ ions are produced by electrospray ionization and observed to be highly stable with very large adiabatic electron detachment energies: 6.25, 6.64, 6.27, and 5.60 eV for X = F, Cl, Br, and I, respectively. Theoretical calculations reveal that the frontier molecular orbitals are mainly of uranyl U−O bonding character in $UO_2F_3^-$, but they are from the ligand valence np lone pairs in the heavier halogen complexes. Extensive bonding analyses are carried out for $UO_2X_3^-$ as well as for the doubly charged tetracoordinate complexes ($UO_2X_4^{2-}$), showing that the U−X bonds are dominated by ionic interactions with weak covalency. The U−X bond strength decreases down the periodic table from F to I. Coulomb barriers and dissociation energies of $UO_2X_4^{2-} \rightarrow UO_2X_3^- + X^-$ are calculated, revealing that all gaseous dianions are in fact metastable. The dielectric constant of the environment is shown to be the key in controlling the thermodynamic and kinetic stabilities of the tetracoordinate uranyl complexes via modulation of the ligand−ligand Coulomb repulsions.

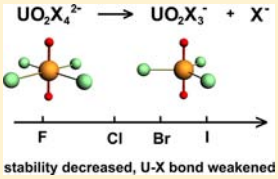

1. INTRODUCTION

Uranyl dication (UO_2^{2+}) is the most stable form of uranium in nature and usually coordinated by ligands or solvent molecules. Investigations of uranyl complexes and their stabilities are important in understanding the chemical transformation and migration of nuclear wastes, as well as the coordination chemistry in recycling spent nuclear fuels.[1] Elucidating the nature of uranium−ligand chemical bonds is critical for evaluating the binding ability of various ligands[2−4] and for development of new ligands for efficient and selective separation of fission products.[5−15] Among numerous uranyl compounds with various inorganic and organic ligands, uranyl halides have been extensively investigated due to their important roles in the extraction of uranium into the aqueous phase as well as in serving as useful starting materials for syntheses of a wide variety of uranium compounds.[16,17]

The uranyl dication is linear with two U≡O triple bonds, $[O{\equiv}U{\equiv}O]^{2+}$, which is typically coordinated by 4−6 ligands in the equatorial plane.[1,18] No isolated uranyl halides with fewer than four equatorial ligands have been observed in the condensed phases.[1] Extended X-ray absorption fine structure (EXAFS) and X-ray crystallography experiments have shown that uranyl usually has a saturated equatorial coordination number (CN_{eq}) of 4−6 by ligands and/or solvent molecules in condensed phases.[19−21] In the solid state, multiply charged uranyl halides, $UO_2F_5^{3-}$ [22] and $UO_2X_4^{2-}$ (X = Cl, Br, I),[23−26] have been observed experimentally. Despite the syntheses of complexes formulated with $UO_2F_6^{4-}$ and $UO_2F_7^{5-}$,[27,28] uranyl halides with more than 6 equatorial halogen ligands seem unlikely as the X-ray structure of the UO_2F_2 crystal shows that the $UO_2F_6^{4-}$ ion has a D_{3d} local symmetry with the six ligands arranged in a nonplanar zigzag crown along the equatorial plane.[29] The multiply charged complexes appear to be less stable in the solution than in the solid due to ligand exchanges. For example, an F^- ligand in the $UO_2F_5^{3-}$ trianion is substituted by a neutral solvent molecule (water or acetonitrile) to form the $UO_2F_4(solvent)^{2-}$ dianions.[30,31] EXAFS and UV−Vis absorption experiments show that the $UO_2Cl_4^{2-}$ dianion exists in organic solutions with high concentrations of Cl^-.[32] The $UO_2Br_4^{2-}$ dianion has been observed to be stable in ionic liquids,[33] whereas high-energy X-ray scattering (HEXS) data have revealed an average U−Br CN_{eq} of 1.9 in concentrated aqueous hydrobromic acid solutions.[23] Uranyl species tend to retain low CN_{eq} in the gas phase due to increased Coulomb repulsion between the ligands. Indeed, uranyl complexes exist in low-temperature noble-gas matrices in the form of neutral UO_2X_2 (X = F, Cl, Br) species.[34−36] Recently, Groenewold et al. measured the infrared multiphoton dissociation spectroscopy (IRMPD) of $UO_2X_3^-$ (X = F, Cl, Br, I) in the gas phase.[13]

Received: March 15, 2013
Published: May 10, 2013

   dx.doi.org/10.1021/ic4006482 | Inorg. Chem. 2013, 52, 6617−6626

We observed stable $UO_2F_4^{2-}$ and $UO_2Cl_4^{2-}$ dianions and their solvation complexes with water and acetonitrile molecules in the gas phase using electrospray ionization (ESI),[37,38] but $UO_2Br_4^{2-}$ and $UO_2I_4^{2-}$ were not observed in these experiments.

The two strong U≡O triple bonds in uranyl are formed between the U 5f/6d orbitals and the O 2p orbitals.[39] The resulting six frontier bonding orbitals (σ_u, π_u, π_g, and σ_g) are fully occupied with 12 valence electrons. The U 7s shell usually does not participate in bonding in uranyl complexes because of its high orbital energy in U(VI); the U 5fδ_u, 5fϕ_u, and 6dδ_g orbitals remain nonbonding because their symmetries do not match with that of the O 2p orbitals. These occupied and nonbonding frontier orbitals are available for σ and π interactions with the equatorial ligands, thus weakening the U≡O bond upon coordination.[18,40] The CN_{eq} in uranyl complexes is a result of competition between the U−X bonding strength and the electrostatic Coulomb repulsion among the negatively charged X ligands. Photodissociation was not observed for $UO_2F_3^-$ in the previous IRMPD experiment,[13] implying that the U−F bond is the strongest among the $UO_2X_3^-$ complexes. Recent experimental observations and investigations of $UO_2X_4^{2-}$ (X = F, Cl) and $UO_2X_3^-$ (X = F, Cl, Br, I) in the gas phase indicate that there are rich chemistries in uranyl halides outside the condensed phases.

Here we report the first gas-phase investigation of the electronic structures of $UO_2X_3^-$ (X = F, Cl, Br, I) using photoelectron spectroscopy (PES) and relativistic quantum chemistry calculations. The ESI-PES technique developed in the Wang lab[41] is uniquely suited to study negatively charged uranyl complexes. In the current study, the PES experiments are carried out on the series of $UO_2X_3^-$ complexes (X = F, Cl, Br, I), which are produced by ESI. We find that all $UO_2X_3^-$ species are highly stable electronically with adiabatic electron detachment energies (ADEs) ranging from 5.60 eV for $UO_2I_3^-$ to as high as 6.64 eV for $UO_2Cl_3^-$. Calculations using density function theory (DFT) and ab initio wave function theory (WFT) are carried out to gain insight into the electronic structures and stabilities of these monoanions. The thermodynamic and kinetic stabilities of the $UO_2X_4^{2-}$ (X = F, Cl, Br, I) dianions are also explored in relation to the $UO_2X_3^-$ monoanions. Extensive bonding analyses are performed to understand the nature of the U−X bonds in $UO_2X_3^-$ and $UO_2X_4^{2-}$.

2. EXPERIMENTAL AND THEORETICAL METHODS

2.1. Electrospray and Photoelectron Spectroscopy. The experiment was performed using the ESI-PES apparatus developed in the Wang lab, as described in detail previously.[41] Briefly, the $UO_2X_3^-$ (X = Cl, Br, I) anions were produced by electrospray of a 1 mM solution of $UO_2(CH_3CO_2)_2{\cdot}2H_2O$ mixed with the corresponding halogen acid (HX) in a methanol/water (90/10) mixed solvent. The pH of the solution was adjusted to be ∼4. The $UO_2F_3^-$ complex was formed by adding an excess amount of AgF to a 1 mM solution of $U(SO_4)_2$ in acetonitrile. Anions from the ESI source were accumulated in an ion trap operated at 20 K for 0.1 s and then pulsed into the extraction zone of a time-of-flight mass spectrometer. Anions of interest were selected by a mass gate and decelerated before being intercepted by a laser beam in the detachment region of a magnetic-bottle photoelectron analyzer. In the current study, we used an F_2 excimer laser (157 nm, 7.866 eV) because of the very high electron binding energies of the uranyl halide complexes. The details of the cryogenically cooled ion trap developed by the Wang lab have been described previously.[42a] Cold ions are essential to eliminate vibrational hot bands and achieve better spectral resolution and more accurate ADE measurements.[42b] PES experiments were calibrated using the known spectra of Au^- and I^-. Au^- atomic anion was produced by ESI of a acetonitrile solution of PPh_3AuCl with $NaSCH_3$ and a trace amount of CH_3OH.[43] The current electron flight tube is shortened from 4.0 to 2.5 m, leading to only a slight decrease of electron energy resolution.[37,38] The electron kinetic energy resolution of the current magnetic-bottle photoelectron analyzer with the shortened electron flight tube was about 3%, i.e., 30 meV for 1 eV electrons.[42b,44]

2.2. Theoretical Methods. Theoretical studies were carried out using both DFT and WFT methods. DFT calculations were performed on both $UO_2X_3^-$ and UO_2X_3 (X = F, Cl, Br, I) using the generalized gradient approximation (GGA) with the PBE exchange-correlation functional[45] as implemented in the Amsterdam Density Functional (ADF 2010.02) program.[46−48] The Slater basis sets with the quality of triple-ζ plus two polarization functions (TZ2P)[49] were used, with the frozen core approximation applied to the inner shells [$1s^2$-$5d^{10}$] for U, [$1s^2$] for O and F, [$1s^2$-$2p^6$] for Cl, [$1s^2$-$3d^{10}$] for Br, and [$1s^2$-$4d^{10}$] for I. The scalar relativistic (SR) and spin−orbit (SO) coupling effects were taken into account by the zero-order regular approximation (ZORA).[50] Geometries were fully optimized at the SR-ZORA level, and single-point energies were calculated with inclusion of the SO effects via the SO-ZORA approach.

To compare with the experimental results, we further carried out ab initio WFT calculations using advanced electron correlation methods implemented in the MOLPRO 2008.1 program.[51] The coupled-cluster with single and double and perturbative triple excitations (CCSD(T)) and complete-active-space self-consistent field (CASSCF) methods were used. Structures of $UO_2X_3^-$ (X = F, Cl, Br, I) were optimized at the level of CCSD(T) with the SR effects included. Single-point CCSD(T) energies of the ground and excited states of UO_2X_3 (X = F, Cl, Br, I) were calculated at the optimized geometries of $UO_2X_3^-$, which accurately generated state-specific SR energies for all states. Electron binding energies corresponding to one-electron transitions from the closed-shell ground state of $UO_2X_3^-$ (X = F, Cl, Br, I) to the ground and excited states of UO_2X_3 were obtained using the CASSCF/CCSD(T)/SO approach, which has been shown to produce highly accurate excitation energies for heavy-element systems.[37,40,52−55] In this approach, SO coupling was accounted for using a state-interacting method with SO pseudopotentials, where SO splittings were determined as a perturbation to the SR state energies and calculated on the basis of CASSCF wave functions with the diagonal matrix elements replaced by the individual CCSD(T) state energies. We also used the CASSCF/CR-EOM-CCSD(T)/SO approach, where CR-EOM-CCSD(T)[56] energies obtained from the EOM-CCSD energies with completely renormalized EOM-CCSD(T) corrections as implemented in NWChem 6.0 were used as the diagonal elements.[57] In this approach, CR-EOM-CCSD(T) calculations were performed on the neutrals at the CCSD(T)-optimized geometry of the monoanions to obtain the energies of the excited states, with the CCSD(T) energy of the state corresponding to one electron removed from the HOMO ($4a_2''$) as reference. In the MOLPRO and NWChem calculations, we used the Stuttgart energy-consistent relativistic 32-valence-electron pseudopotentials ECP60MWB (U) and the corresponding ECP60MWB-SEG basis for U,[58−60] the valence triple-ζ basis sets aug-cc-pVTZ for O, F, and Cl,[61,62] the relativistic 25-valence-electron pseudopotential ECP10MDF (Br) and the corresponding aug-cc-pVTZ-PP basis set for Br,[63] and the relativistic 25-valence-electron pseudopotential ECP28MDF and the corresponding aug-cc-pVTZ-PP basis set for I.[64]

For dissociation of $UO_2X_4^{2-} \rightarrow UO_2X_3^- + X^-$, we did DFT/B3LYP calculations[65,66] for the equilibrium geometries and vibrational spectra of the reactants, transition states, and products using Gaussian 09.[67] Basis sets used for O and X were the valence double-ζ basis sets aug-cc-pVDZ.[61−64] Zero-point energies (ZPE) and free energy corrections were derived from the B3LYP frequency calculations. Single-point energies of the structures optimized at the B3LYP level were calculated using the CCSD(T) method with the same basis sets. Natural localized molecular orbitals (NLMO), natural population analyses, and natural resonance theory (NRT) bond order were calculated to understand the bonding and electronic structures of $UO_2X_4^{2-}$ and $UO_2X_3^-$ based

dx.doi.org/10.1021/ic4006482 | Inorg. Chem. 2013, 52, 6617−6626

on the B3LYP results using the natural bond orbital method,[68] implemented in the NBO 5.G program.[69] Linear transit (LT) calculations were performed by constrained optimizations at each LT coordinate along the $X^-\cdots UO_2X_3^-$ dissociation pathway using the DFT/PBE method at the SR level in ADF 2010.02.[46] Further bonding analyses were performed with the energy decomposition approach (EDA) to evaluate the relative importance of steric repulsion and the ionic and covalent bonding effects.[70−72]

3. EXPERIMENTAL RESULTS

The 157 nm PES spectra of $UO_2X_3^-$ (X = F, Cl, Br, I) at 20 K are shown in Figure 1. The extremely high electron binding energies of these species made it necessary for us to use the highest photon energy available in our lab at 157 nm, in particular for $UO_2F_3^-$ and $UO_2Cl_3^-$.

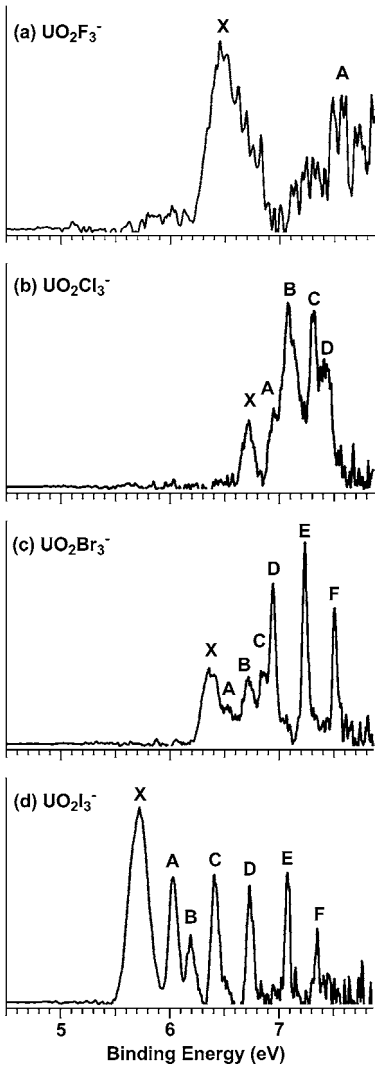

Figure 1. Photoelectron spectra of (a) $UO_2F_3^-$, (b) $UO_2Cl_3^-$, (c) $UO_2Br_3^-$, and (d) $UO_2I_3^-$ at 20 K and 157 nm (7.866 eV).

3.1. $UO_2F_3^-$. We found it to be extremely challenging to obtain the spectrum of $UO_2F_3^-$ because of its low detachment cross sections. Despite relatively strong ion intensities, very weak photoelectron signals were observed for $UO_2F_3^-$ at 157 nm. The spectrum displayed in Figure 1a was accumulated for more than 20 h, but it still displays relatively poor signal-to-noise ratios, especially at high binding energies above 7 eV. A broad band was observed around 6.5 eV (X). The poor signal-to-noise ratios prevented us from definitively assigning detachment transitions at higher binding energies. A band labeled as A was tentatively identified for the sake of discussion. Because of the elimination of vibrational hot bands, a relatively sharp onset was observed for the ground state band X, allowing us to measure the ADE or the electron affinity of neutral UO_2F_3 as 6.25 ± 0.05 eV. This quantity was obtained by drawing a straight line along the leading edge of the X band and then adding the instrumental resolution (0.05 eV) to the intersection with the binding energy axis. The vertical detachment energy (VDE) for band X was measured to be 6.53 ± 0.05 eV from the band maximum. The ADE and VDE for the X band are given in Table 1, where they are compared with the theoretical results.

Table 1. Observed and Calculated Adiabatic (ADE) and Vertical (VDE) Detachment Energies for $UO_2X_3^-$ (X = F, Cl, Br, I)[a]

			DFT/PBE		CCSD(T)[d]	
		exp[b]	SR	SO	SR	SO[c]
$UO_2F_3^-$	ADE	6.25 (5)	5.44	5.31	6.48	6.35
	VDE	6.53 (5)	5.62	5.52	6.81	6.71
$UO_2Cl_3^-$	ADE	6.64 (5)	5.47	5.41	6.82	6.76
	VDE	6.72 (5)	5.52	5.47	6.88	6.83
$UO_2Br_3^-$	ADE	6.27 (5)	5.24	5.18	6.45	6.39
	VDE	6.37 (5)	5.24	5.18	6.45	6.39
$UO_2I_3^-$	ADE	5.60 (5)	4.84	4.71	5.86	5.73
	VDE	5.72 (5)	4.85	4.72	5.86	5.73

[a]All energies are in eV. [b]Numbers in parentheses represent the experimental uncertainties in the last digit. [c]These SO results are estimated using the SR CCSD(T) energies with the ad hoc SO corrections from the DFT/PBE calculations. [d]Optimized geometries of the $UO_2X_3^-$ (X = Br, I) anions and their neutrals are so close that the calculated ADEs and VDEs are nearly identical, respectively.

3.2. $UO_2X_3^-$ (X = Cl, Br, I). Better spectra were obtained for the heavier halogen complexes, $UO_2X_3^-$ (X = Cl, Br, I), each with well-resolved spectral features, as shown in Figure 1b−d, respectively. The $UO_2Cl_3^-$ complex exhibits the highest electron binding energies with five resolved detachment transitions (X, A−D). The ADE and VDE of the X band for $UO_2Cl_3^-$ were measured to be 6.64 and 6.72 eV, respectively. Electron binding energies decrease systematically from $UO_2Cl_3^-$ to $UO_2I_3^-$. In addition, more and sharper spectral features were observed for the heavier complexes, probably as a result of the SO splitting from detachment of the heavier halogen ligand orbitals. The ADE and VDE for the first bands for all $UO_2X_3^-$ complexes are given in Table 1, where they are compared with theoretical results at different levels of theory. The VDEs for all detachment features are given in Tables 2 and 3, where they are compared with theoretical calculations from CASSCF/CCSD(T)/SO.

4. THEORETICAL RESULTS

4.1. Structures of $UO_2X_3^-$ and UO_2X_3 (X = F, Cl, Br, I). Optimized ground state structural parameters and U−O symmetric vibrational frequencies for $UO_2X_3^-$ and UO_2X_3 (X = F, Cl, Br, I) at the SR level are given in Table 4. Upon electron detachment from $UO_2X_3^-$, both DFT and CCSD(T) calculations indicate that the U−X bond lengths decrease as a result of the reduced intramolecular Coulomb repulsion, but the change becomes smaller from X = F to I, suggesting the intramolecular Coulomb repulsion becomes weaker in the

dx.doi.org/10.1021/ic4006482 | Inorg. Chem. 2013, 52, 6617−6626

Table 2. VDEs Observed and Calculated at the CASSCF/CCSD(T)/SO Level with the Corresponding MOs of $UO_2X_3^-$ (X = F, Cl)[a]

$UO_2F_3^-$				$UO_2Cl_3^-$			
obs features	VDE (expt)[b]	MO (SR)	VDE (theor)	obs features	VDE (expt)[b]	MO (SR)	VDE (theor)
X	6.53 (5)	$4a_2''$ (U−O σ_u)	6.69	X	6.72 (5)	$4a_2''$ (Cl 3p)	6.83
A	∼7.5	$5e'$ (U−O π_u)	7.55	A	6.95 (5)	$2e''$ (Cl 3p)	7.00
		$2e''$ (U−O π_g)	7.91			$2e''$ (Cl 3p)	7.00
		$2e''$ (U−O π_g)	7.92	B	7.08 (5)	$5e'$ (Cl 3p)	7.04
		$5e'$ (U−O π_u)	8.14	C	7.31 (5)	$5e'$ (Cl 3p)	7.25
		$5a_1'$ (U−O σ_g)	8.33	D	7.41 (5)	$1a_2'$ (Cl 3p)	7.27
		$4e'$	8.87			$4e'$ (Cl 3p)	7.85
		$4e'$	8.94			$4e'$ (Cl 3p)	7.91
		$1a_2'$	9.16			$5a_1'$ (Cl 3p)	8.13
		$3a_2''$	9.28			$3a_2''$	8.45
		$3e'$	9.72			$3e'$	9.25
		$3e'$	9.75			$3e'$	9.46
		$1e''$	9.94			$4a_1'$	9.90
		$1e''$	9.95			$1e''$	10.10
		$4a_1'$	10.24			$1e''$	10.14

[a]All energies are in eV. [b]The numbers in parentheses represent the experimental uncertainties in the last digit.

Table 3. VDEs Observed and Calculated at the CASSCF/CCSD(T)/SO Level with the Corresponding MOs of $UO_2X_3^-$ (X = Br, I)[a]

$UO_2Br_3^-$				$UO_2I_3^-$			
obs features	VDE (expt)[b]	MO (SR)	VDE (theor)	obs features	VDE (expt)[b]	MO (SR)	VDE (theor)
X	6.37 (5)	$2e''$ (Br 4p)	6.35	X	5.72 (5)	$2e''$ (I 5p)	5.62
		$4a_2''$ (Br 4p)	6.36			$2e''$ (I 5p)	5.63
		$2e''$ (Br 4p)	6.38			$4a_2''$ (I 5p)	5.71
A	6.53 (5)	$5e'$ (Br 4p)	6.64	A	6.03 (5)	$5e'$ (I 5p)	5.97
B	6.71 (5)	$1a_2'$ (Br 4p)	6.67	B	6.20 (5)	$1a_2'$ (I 5p)	6.07
C	6.86 (5)	$5e'$ (Br 4p)	6.79	C	6.41 (5)	$4e'$ (I 5p)	6.30
D	6.94 (5)	$4e'$ (Br 4p)	7.16	D	6.73 (5)	$5e'$ (I 5p)	6.58
E	7.24 (5)	$4e'$ (Br 4p)	7.43	E	7.08 (5)	$4e'$ (I 5p)	6.97
F	7.51 (5)	$5a_1'$ (Br 4p)	7.70	F	7.35 (5)	$5a_1'$ (I 5p)	7.25
		$3a_2''$	8.38			$3a_2''$	8.46
		$3e'$	9.37			$3e'$	9.53
		$3e'$	9.62			$3e'$	9.80
		$4a_1'$	9.98			$4a_1'$	10.10
		$1e''$	10.21			$1e''$	10.37
		$1e''$	10.25			$1e''$	10.41

[a]All energies are in eV. [b]Numbers in parentheses represent the experimental uncertainties in the last digit.

Table 4. Optimized Ground State (GS) Geometrical Parameters, Symmetries (Sym), and U−O Stretching Vibrational Frequencies (ν_s) for $UO_2X_3^-$ and UO_2X_3 (X = F, Cl, Br, I) at the Scalar-Relativistic Level

			DFT/PBE			CCSD(T)	
complexes	sym	GS	U−O/Å	U−X/Å	ν_s(U−O)/cm^{-1}	U−O/Å	U−X/Å
$UO_2F_3^-$	D_{3h}	$^1A_1'$	1.819	2.165	807	1.782	2.160
UO_2F_3	D_{3h}	$^2A_2''$	1.814	2.083	783	1.794	2.055
$UO_2Cl_3^-$	D_{3h}	$^1A_1'$	1.794	2.632	834	1.757	2.638
UO_2Cl_3	D_{3h}	$^2A_2''$	1.783	2.580	846	1.751	2.571
$UO_2Br_3^-$	D_{3h}	$^1A_1'$	1.789	2.803	840	1.752	2.796
UO_2Br_3	D_{3h}	$^2E''$	1.782	2.804	861	1.751	2.786
$UO_2I_3^-$	D_{3h}	$^1A_1'$	1.785	3.028	845	1.748	3.015
UO_2I_3	D_{3h}	$^2E''$	1.780	3.025	862	1.748	3.000

heavier complexes. At the DFT level, U−O bond lengths in neutral UO_2X_3 are all predicted to be slightly decreased. However, at the CCSD(T) level, U−O bonds in UO_2F_3 are increased by 0.012 Å whereas U−O bonds in the three heavier halogen complexes are unchanged or decreased slightly. CCSD(T) results are consistent with the trend of the U−O symmetrical stretching frequencies at the DFT/PBE level, suggesting weakened U−O bonding in neutral UO_2F_3 but

dx.doi.org/10.1021/ic4006482 | Inorg. Chem. 2013, 52, 6617−6626

strengthened U−O bonding in the heavier UO_2X_3 complexes. The U−O bond length change for UO_2F_3 at the DFT/PBE level is due to the fact that DFT calculations often overestimate the effects of the intramolecular Coulomb repulsion on the U−O bond lengths in the uranyl halogen complexes.[37,38]

4.2. Calculated First ADEs and VDEs for $UO_2X_3^-$ (X = F, Cl, Br, I). The first ADEs and VDEs for $UO_2X_3^-$ (X = F, Cl, Br, I) calculated at the DFT/PBE and CCSD(T) levels of theory are compared with the experimental data in Table 1. Overall, the DFT/PBE methods significantly underestimate the electron binding energies for the $UO_2X_3^-$ complexes by about 0.7−1.2 eV. These large discrepancies between DFT calculations and experimental ADEs/VDEs have been observed recently for other uranium-containing mono- and dianions.[37,38,73] When the neutral molecule has an open-shell configuration that can undergo first-order SO splitting while the monoanion has a closed-shell configuration without first-order SO splitting, the ADEs and VDEs are usually overestimated by the SR formalism relative to the SO formalism.[74] At the DFT/PBE level, the calculated SO effects for the ADEs and VDEs of $UO_2F_3^-$ and $UO_2I_3^-$ are about 0.10−0.13 eV and about 0.05−0.06 eV for those of $UO_2Cl_3^-$ and $UO_2Br_3^-$, as shown in Table 1. The poor performance of the DFT method for the ADEs and VDEs is due to its overestimation of the electrostatic Coulomb repulsion for the anions. The CCSD(T) results agree well with the experimental data (Table 1). For $UO_2X_3^-$, the calculated SR CCSD(T) VDEs are already in good agreement with the experiment, overestimating the ADEs only by about 0.2−0.3 eV, as also found in the cases of $UO_2F_4^{2-}$ and $UO_2Cl_4^{2-}$ recently.[37,38] Using the SO corrections from the PBE calculations and the SR CCSD(T) results, the estimated ADEs and VDEs for $UO_2X_3^-$ are in much better agreement with the experimental data (Table 1).

Calculated VDEs for all MOs at the CASSCF/CCSD(T)/SO level are compared with the experimental data in Tables 2 and 3. Complete results of the CR-EOM-CCSD(T) calculations are summarized in Tables S1 and S2, Supporting Information. The VDEs calculated from the two methods are largely consistent with each other.

4.3. Molecular Orbital Analyses and SO Effects for $UO_2X_3^-$ (X = F, Cl, Br, I). Figure 2 shows the occupied MO levels of primarily ligand valence *n*p character for $UO_2X_3^-$ (X = F, Cl, Br, I) at the SR and SO levels. The frontier MOs of $UO_2F_3^-$ exhibit U−O bonding characters, which are highlighted in light blue color. Calculated VDEs for all MOs by DFT/PBE are given in Tables S3 and S4, Supporting Information. U−O bonding characters of the occupied frontier MOs in $UO_2F_3^-$ are indicated, whereas frontier MOs of $UO_2X_3^-$ (X = Cl, Br, I) are all of halogen *n*p characters. The isocontour surfaces of the occupied MOs for $UO_2F_3^-$ and $UO_2Cl_3^-$ from SR-DFT/PBE calculations are presented in Figures 3 and 4, respectively. The MO pictures for $UO_2Br_3^-$ and $UO_2I_3^-$ (not shown) are similar to those of $UO_2Cl_3^-$. We also observed recently that the frontier occupied MOs in $UO_2F_4^{2-}$ are of U−O bonding character, while those in $UO_2Cl_4^{2-}$ are of Cl 3p character.[37,38] A MO correlation diagram is shown in Figure 5 for $UO_2Cl_3^-$ at the SR-DFT level, as a representative for the heavier $UO_2X_3^-$ complexes. The U−O bonding orbitals are clearly lower in energy than those from the *n*p valence orbitals of the ligand, and there is a large energy gap between the occupied MOs and the unoccupied 5f-type MOs.

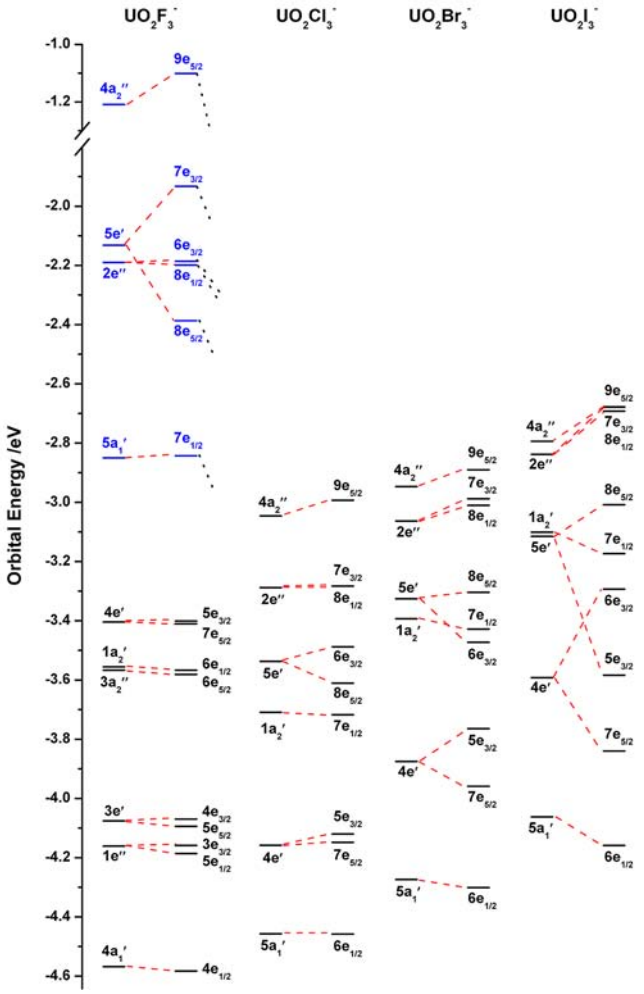

Figure 2. SR and SO molecular orbital (MO) energy levels of $UO_2X_3^-$ with primarily ligand *n*p valence orbitals by DFT/PBE calculations, where the $4a_2''$ orbital is the HOMO. Note the energy levels of $UO_2F_3^-$ in blue are primarily U−O bonding orbitals, and the SR and SO MO energy levels of $UO_2F_3^-$ are shifted up by 1.3 eV as a whole for better comparison.

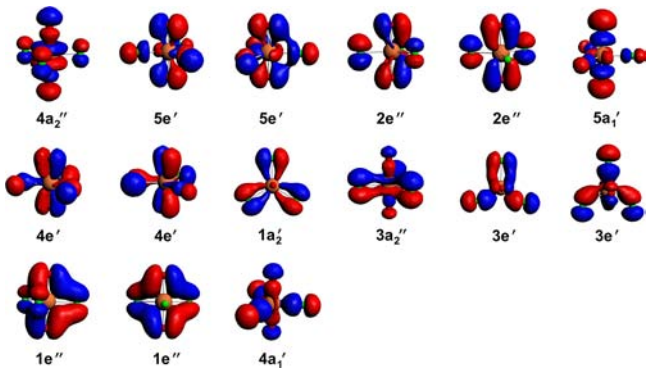

Figure 3. Contour plots of the occupied valence MOs of $UO_2F_3^-$ at the DFT/PBE level; $4a_2''$ orbital is the HOMO.

Figure 2 shows that the SO effects in the ligand *n*p MOs increase significantly from F to I, consistent with the fact that the differential SO effects are proportional to Z^4 (Z is the atomic number).[75] In particular, the 4e′ and 5e′ orbitals in $UO_2X_3^-$ (X = Cl, Br, I) display stronger SO effects due to contributions of U 6p orbitals, as shown in other uranium(VI)

dx.doi.org/10.1021/ic4006482 | Inorg. Chem. 2013, 52, 6617−6626

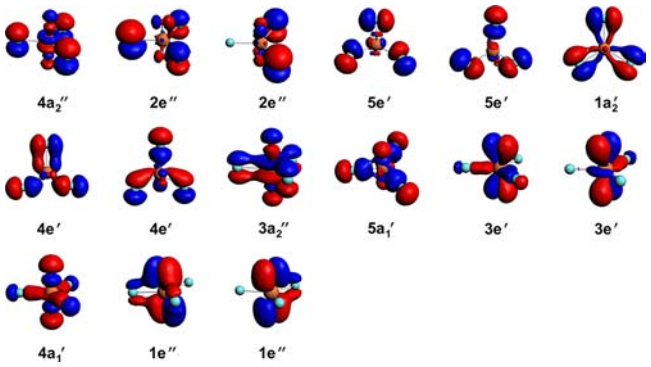

Figure 4. Contour plots of the occupied valence MOs of $UO_2Cl_3^-$ at the DFT/PBE level; $4a_2''$ orbital is the HOMO.

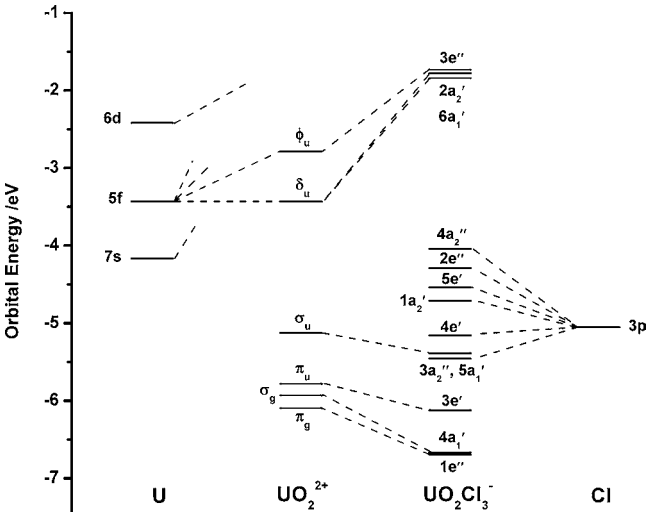

Figure 5. MO energy levels of $UO_2Cl_3^-$ at the SR-DFT/PBE level; $4a_2''$ orbital is the HOMO, and $6a_1'$ orbital is the LUMO.

compounds.[76,77] On the other hand, SO effects are negligible for the F 2p-type orbitals, while the 5e′ U−O bonding orbital in $UO_2F_3^-$ exhibits a large SO effect.

5. INTERPRETATION OF THE PHOTOELECTRON SPECTRA OF $UO_2X_3^-$

5.1. $UO_2F_3^-$. Calculated VDEs presented in Table 2 show that the first six detachment channels for $UO_2F_3^-$ are from MOs of U−O bonding character (Figure 2). The HOMO ($4a_2''$) of $UO_2F_3^-$ is mainly from the σ_u orbital of UO_2^{2+} with slight antibonding interactions with the F $2p_z$ orbitals (Figure 3). The calculated first VDE of 6.69 eV at the CASSCF/CCSD(T)/SO level agrees well with the experimental result of 6.53 eV. The CCSD(T) structural parameters given in Table 4 indicate that upon electron detachment from the HOMO the U−O bond lengths increase by 0.012 Å and the U−F bond lengths decrease by 0.105 Å in neutral UO_2F_3. These large geometry changes are consistent with the broad ground state band (X) in the PES spectrum of $UO_2F_3^-$ (Figure 1a). Calculated VDEs for the second to the fourth detachment channels are from the U−O π_u (5e′) and U−O π_g (2e″) MOs with calculated VDEs from 7.55 to 7.92 eV. Considering the fact that the first VDE was overestimated by 0.16 eV, we suspect that all three detachment channels should be accessible at the 157 nm detachment energy and contribute to the signals observed in the higher binding energy side in the spectrum of $UO_2F_3^-$ (Figure 1a). Unfortunately, the signal-to-noise ratios in the high binding energy side are too poor to allow any definitive assignments.

5.2. $UO_2Cl_3^-$. Calculated VDEs at the CASSCF/CCSD(T)/SO level and assignments for the PES features of $UO_2Cl_3^-$ are also given in Table 2. In contrast to $UO_2F_3^-$, the frontier occupied MOs of $UO_2Cl_3^-$ all have Cl 3p character (Figure 4), which are responsible for the top nine detachment channels. The VDEs for detachment from the U−O bonding orbitals have binding energies above 8.4 eV, too high to be accessed at 157 nm. Thus, all detachment bands observed for $UO_2Cl_3^-$ in Figure 1b should be due to the Cl 3p ligand orbitals. In comparison, the detachment features observed for $UO_2F_3^-$ are all from U−O bonding orbitals, which explains the low detachment cross sections for the fluoride complex. In a recent study on UF_6^-,[73] we found that its detachment cross section at 157 nm for the U 5f HOMO was so small that we could not obtain its photoelectron spectrum.

The HOMO ($4a_2''$) of $UO_2Cl_3^-$ has π antibonding character between the Cl $3p_z$ orbitals and the U−O σ_u orbital (Figure 4). Detachment from this MO gives rise to the X band in the PES spectra (Figure 1b). Calculated VDE of 6.83 eV is in good agreement with the experimental value of 6.72 eV (Table 2). Upon electron detachment, there is only a small contraction (0.067 Å) of the U−Cl bonds in neutral UO_2Cl_3 based on the CCSD(T) calculation (Table 4), consistent with the relatively sharp X band. The second detachment channel is from the 2e″ orbital, which is mainly of Cl $3p_z$ character. The SO effect is negligible for this MO (Figure 2), and calculated VDEs of 7.00 eV for both SO channels are in good agreement with the 6.95 eV VDE measured for band A (Table 2). Bands B and C are in excellent agreement with the calculated VDEs of the SO split 5e′ orbitals, whereas band D corresponds to detachment from the $1a_2'$ orbital. The VDEs for the two remaining Cl 3p-based ligand orbitals, 4e′ and $5a_1'$ (Table 2), are too high to be accessed at 157 nm.

5.3. $UO_2X_3^-$ (X = Br and I). PES spectra of $UO_2Br_3^-$ and $UO_2I_3^-$ are very similar to each other (Figure 1); MOs of the two heavier halogen complexes are similar to those of $UO_2Cl_3^-$, as shown in Figure 4. PES spectra in Figure 1 reveal that electron binding energies of $UO_2Cl_3^-$ are the highest and decrease from Cl to I. The major difference between the PES spectra of the two heavier complexes and that of $UO_2Cl_3^-$ is the SO effects (Figure 2), which are responsible for the well-resolved PES spectral features for the Br and I complexes. Detailed spectral assignments for these two complexes are given in Table 3, which shows that, because of the reduced electron binding energies, all PES bands are due to the ligand-based valence MOs, while the U−O-based MOs all have too high binding energies to be accessed at 157 nm.

CASSCF/CCSD(T)/SO calculations indicate that the VDEs for the top two MOs (2e″ and $4a_2''$) for $UO_2Br_3^-$ and $UO_2I_3^-$ are very close in each system (Table 3), in excellent agreement with the broad X band in both spectra. Except for the C and D bands, all higher binding energy features for both systems also have a one-to-one correspondence, as shown in Table 3. In general, the calculated VDEs for $UO_2I_3^-$ are in very good agreement with the experimental data with discrepancies within 0.1 eV. Calculated VDEs for the higher detachment channels for $UO_2Br_3^-$ display a slightly larger error (~0.2 eV) in comparison with the experimental data.

5.4. Inadequacy of DFT GGA Energies and Importance of Spin−Orbit Effects. The ADEs of $UO_2X_3^-$ (X = F, Cl, Br,

dx.doi.org/10.1021/ic4006482 | Inorg. Chem. 2013, 52, 6617−6626

Table 5. Theoretical Analyses of the U−X Bonds in $UO_2X_3^-$ and $UO_2X_4^{2-}$ (X = F, Cl, Br and I) at the DFT/B3LYP Level[a]

				NLMO				
	U−X/Å	Q(U)	Q(X)	σ	π	BO_{N-M}	BO_{NRT}	Cov.(NRT)
$UO_2X_3^-$								
F	2.161	2.15	−0.63	9.1% U($s^{0.24}p^{0.01}d^{1.89}f$) + 90.8% F($sp^{1.82}$)	5.5% U($d^{0.81}f$) + 94.4% F(p)	1.549	1.026	9.0%
Cl	2.650	1.61	−0.48	14.2% U($s^{0.76}d^{2.33}f$) + 85.5% Cl($sp^{2.55}$)	7.3% U($d^{1.15}f$) + 92.6% Cl(p)	1.429	0.965	15.1%
Br	2.813	1.52	−0.45	15.3% U($s^{0.97}d^{2.62}f$) + 84.3% Br($sp^{3.52}$)	7.7% U($d^{1.24}f$) + 92.1% Br(p)	1.411	0.990	16.3%
I	3.043	1.42	−0.42	16.9% U($s^{1.31}d^{3.09}f$) + 82.5% I($sp^{4.55}$)	7.9% U($d^{1.37}f$) + 91.9% I(p)	1.384	0.952	19.0%
$UO_2X_4^{2-}$								
F	2.236	2.05	−0.66	8.5% U($s^{0.20}d^{1.03}f$) + 91.4% F($sp^{1.35}$)	4.8% U($d^{0.79}f$) + 95.1% F(p)	1.452	0.994	10.2%
Cl	2.755	1.43	−0.55	13.1% U($s^{0.51}d^{1.52}f$) + 86.6% Cl($sp^{2.14}$)	5.4% U($d^{1.00}f$) + 94.2% Cl(p)	1.263	0.990	15.5%
Br	2.922	1.34	−0.53	14.3% U($s^{0.63}p^{0.01}d^{1.71}f$) + 85.3% Br($sp^{3.07}$)	5.8% U($d^{1.06}f$) + 94.2% Br(p)	1.236	0.988	16.9%
I	3.166	1.27	−0.51	15.9% U($s^{0.81}p^{0.01}d^{2.00}f$) + 83.7% I($sp^{4.13}$)	5.6% U($d^{1.11}f$) + 94.3% I(p)	1.182	0.983	18.3%

[a]U−X: U−X bond lengths. Q(U) and Q(X): natural charges on atoms U and O, respectively. NLMO: natural localized molecular orbitals. BO_{N-M}: Nalewajski−Mrozek (N−M) bond order with the trace $(\Delta P)^2$ as N−M bond index referred to as a 4-index set. BO_{NRT}: natural resonance theory bond orders. Cov.(NRT): contribution of covalency to the BO_{NRT}.

I) or the electron affinities of the corresponding neutral UO_2X_3 are very large (Table 1), suggesting that the $UO_2X_3^-$ monoanions are electronically highly stable gaseous species. The ADE of $UO_2Cl_3^-$ is the highest in the series, consistent with the fact that the electron affinity of Cl is the highest among the halogen atoms. The $UO_2X_3^-$ species can be considered as a new class of superhalogens,[78] because their ADEs far exceed those of the halogen anions. DFT calculations with approximate GGA exchange-correlation functionals significantly underestimate the electronic stabilities of the $UO_2X_3^-$ complexes by about 0.7−1.2 eV, as shown in Table 1. This result is consistent with previous findings that GGA functionals usually underestimate VDEs and ADEs and hybrid functionals tend to improve the agreement with experiment.[79] High-level ab initio calculations like CCSD(T) are thus needed.[38] Without SO corrections, even the CCSD(T) calculations at the SR level overestimate the first ADEs by about 0.2−0.4 eV. Using the SO corrections from the DFT/PBE calculations to the SR CCSD(T) results, the resulting ADEs agree much better with the experimental data with an error of ∼0.1 eV (Table 1). Such an ad hoc SO correction to the VDEs (Table 1) also gives results that are comparable to those from the more accurate CASSCF/CCSD(T)/SO calculations (Tables 2 and 3). These results suggest that SO corrections from DFT calculations can be used as initial estimates of the SO effects for the more expensive ab initio calculations.

6. U−X BONDING IN $UO_2X_3^-$ (X = F, Cl, Br, I)

The bonding interactions between U(VI) and the halogen ligands have been extensively investigated both theoretically[5−8] and experimentally.[9−14] To understand the relative roles of the U 7s, 6p, 5f, and 6d orbitals and their chemical bonding with the halogen ligands, we have done a series of theoretical analyses on the uranyl halide complexes, $UO_2X_3^-$ and $UO_2X_4^{2-}$, as shown in Table 5. This table presents the U−X bond lengths at the B3LYP level, natural charges, natural localized molecular orbitals (NLMOs), bond order analyses by the Nalewajski−Mrozek method (BO_{N-M}),[80] natural resonance theory (NRT) (BO_{NRT}), and covalency contributions to the BO_{NRT} [Cov.(NRT)].[81−83] B3LYP U−X bond lengths given in Table 5 are consistent with those from the CCSD(T) calculations in Table 4. Natural population analysis[84] reveals that U carries a large positive charge and the halogen ligands carry considerable negative charges in these U(VI) complexes, indicating that the U−X bonds are mainly due to ionic interactions. Our EDA results for $UO_2X_3^- \rightarrow UO_2^{2+} + X_3^{3-}$ (Table 6) show that while the Pauli repulsion and covalent orbital interactions change slightly from X = F to I, the electrostatic ionic interactions are the major contributions to the total bonding energies, consistent with the ionic character of the U−X bonds. NRT analyses show that $UO_2X_3^-$ can be described by a dominant Lewis resonance structure (DLRS) with a single U−X bond, and the DLRS weight amounts to 56%, 58%, 52%, and 56% for $UO_2X_3^-$ (X = F, Cl, Br, and I, respectively). BO_{NRT} values of U−X are between 1.03 and 0.95, with covalent contributions between 9.0% and 19.0%. BO_{N-M} values are larger than the BO_{NRT} values by ∼0.46 systematically as the former contains partial ionicity. Of particular importance is the trend that when the halogen ligands become heavier, the U−X bond order and total binding energies (Table 6) generally decrease but with increased covalency. This opposite trend indicates that enhanced covalency of the U−X bonds from X = F to I does not indicate stronger bonding because the U−X bonds are dominated by ionic bonding that gradually decreases from X = F to I.

Table 6. Energy Decomposition Analyses (EDA) for $UO_2X_3^- \rightarrow UO_2^{2+} + X_3^{3-}$ (X = F, Cl, Br, I) from DFT/PBE calculations. All energies are in eV

	steric interaction					
X	electrostatic	Pauli	sum[a]	orbital interaction	total bonding energy	steric %[b]
F	−44.67	12.60	−32.07	−10.59	−42.66	75.2%
Cl	−36.26	10.54	−25.72	−9.73	−35.45	72.6%
Br	−33.03	9.52	−23.50	−10.00	−33.51	70.1%
I	−29.40	8.27	−21.13	−10.43	−31.56	67.0%

[a]Steric interaction is the sum of electrostatic and Pauli interactions. [b]Percentage of steric interaction in total bonding energy.

In addition, calculated NLMOs reveal that U−X bonding has very weak σ character between U dfσ and X spσ hybrid orbitals and π-type conjugation interactions between the U dfπ and the X pπ orbitals. As observed in other uranium halogen compounds,[6,8] the U 6d contribution in the U−X bonding increases from X = F to I, showing the important role of the U 6d participation for covalent interactions. There is also significant participation of U 5fδ and 5fϕ orbitals in the U−X bonding, as is the case of $UO_2(HCO_3)_3^-$.[85] The increase of the

dx.doi.org/10.1021/ic4006482 | Inorg. Chem. 2013, 52, 6617−6626

U−X bond covalency from X = F to I to a large extent comes from the better energy level matching between the U 6d and the X sp orbitals. Overall, the U−X bonding of $UO_2X_3^-$ is strongest for X = F and becomes weaker for X = Cl, Br, I, consistent with the conclusions from the previous IRMPD experiemnt.[13] In $UO_2F_4^{2-}$ and $UO_2F_3^-$ species, U−O orbitals are destabilized to become the frontier occupied MOs through mixing with the F 2p orbitals because the fluorine ligands have very low orbital energies in comparison with oxygen. In contrast, U−O orbitals are stabilized so that they lie below the halogen lone-pair orbitals in the heavier $UO_2X_3^-$ (X = Cl, Br, I) species.

7. STABILITY OF $UO_2X_4^{2-}$: COULOMB REPULSION VS U−X BONDING STRENGTH

We recently observed and studied two tetrahalide dianion complexes, $UO_2X_4^{2-}$ (X = F, Cl).[37,38] However, we were not able to observe $UO_2Br_4^{2-}$ and $UO_2I_4^{2-}$ even at very low temperatures. To understand the stability of $UO_2X_4^{2-}$, we calculated the linear transit (LT) energy curves for $X^-\cdots UO_2X_3^- \rightarrow UO_2X_3^- + X^-$, as shown in Figure 6. There

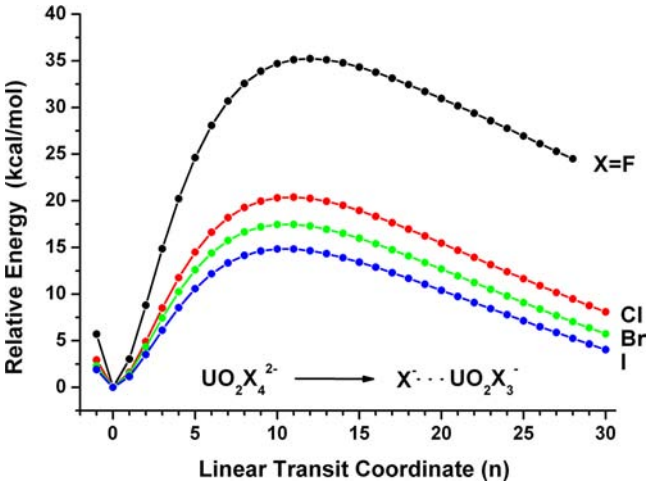

Figure 6. Linear transit (LT) energy curves illustrating dissociation of $UO_2X_4^{2-} \rightarrow UO_2X_3^- + X^-$ (X = F, Cl, Br, I). Energies are obtained from DFT/PBE calculations. $X^-\cdots UO_2X_3^-$ distance $R_n = R_0 + 0.2n$ (n = −1, 0, 1, ..., 30), where R_0 = 2.234, 2.734, 2.910, and 3.143 Å for X = F, Cl, Br, and I, respectively.

is a Coulomb barrier for dissociation to two negative charges, similar to electron detachment from a multiply charged anion.[86,87] Figure 6 shows that the Coulomb barrier decreases from X = F to I, suggesting that the dynamic stability of $UO_2X_4^{2-}$ decreases in the same direction. Table 7 lists the activation energies (E_a), reaction energies (ΔE), and reaction free energies (ΔG) from both B3LYP and CCSD(T) calculations, showing that the dissociation reactions are highly exothermic and all $UO_2X_4^{2-}$ complexes are thermodynamically unstable. Therefore, all $UO_2X_4^{2-}$ species are only kinetically stable (metastable), and their lifetimes are dependent on the barrier heights. The lower barriers and relatively high exothermicity of the dissociation reactions probably made $UO_2X_4^{2-}$ (X = Br and I) too fragile to be observed experimentally.

Coulomb barriers and stabilities of $UO_2X_4^{2-}$ are determined by the balance between the short-range U−X bonding and the long-range Coulomb repulsion between X^- and $UO_2X_3^-$, also similar to the electronic stability of multiply charged anions.[88] Theoretical analyses of the U−X bonds in $UO_2X_4^{2-}$ are also given in Table 5, which shows that the U−X bonding patterns are very similar to those in $UO_2X_3^-$. However, the U−X bonding in $UO_2X_4^{2-}$ is weaker, as can be seen in their longer U−X bond lengths, due to the intramolecular Coulomb repulsion in the dianion complexes. Therefore, the competition between the U−X bond strength and the Coulomb repulsions determines the dynamic stabilities of $UO_2X_4^{2-}$. Because of the ionic nature of the U−X bonds, the dielectric constants (ε_0) of the medium should be critical in determining the stability of the $UO_2X_4^{2-}$ dianion complexes. Our preliminary calculations on dissociation of $UO_2F_4^{2-} \rightarrow UO_2F_3^- + F^-$ show that in the gas phase (ε_0 = 1) $UO_2F_4^{2-}$ is metastable with ΔE = −19.7 kcal/mol. However, in aqueous solution (ε_0 = 80) $UO_2F_4^{2-}$ is highly stable with ΔE = 24.5 kcal/mol. Thus, less X^- ligands can be accommodated in the equatorial plane of uranyl in the gas phase than in the condensed phase because of the increased Coulomb repulsion in the former.

8. CONCLUSIONS

Photoelectron spectroscopy and relativistic quantum chemistry are used to probe the stabilities of gaseous $UO_2X_3^-$ (X = F, Cl, Br, I) and their electronic structures. Low-temperature photoelectron spectra of all four $UO_2X_3^-$ complexes are obtained at 20 K, and the uranyl trihalides are observed to be electronically highly stable with extremely high electron binding energies. The frontier occupied MOs in $UO_2F_3^-$ are shown to mainly consist of U−O bonding orbitals, very different from those in the heavier $UO_2X_3^-$ (X = Cl, Br, I) species, which consist of primarily ligand np-type valence orbitals. DFT calculations are shown to give poor results due to its overestimation of the Coulomb repulsion in $UO_2X_3^-$, whereas CCSD(T) calculations with inclusion of SO effects are in good agreement with the experimental data. Sytematic analyses of the U−X bonding in $UO_2X_3^-$ and $UO_2X_4^{2-}$ (X = F, Cl, Br, I) show that the U−X bonds are dominated by ionic interactions with weak covalency, which increases from X = F to I. Further calculations reveal that the gaseous doubly charged $UO_2X_4^{2-}$

Table 7. Activation Energies (E_a), Reaction Energies (ΔE), and Reaction Free Energies (ΔG) (in kcal/mol) for $UO_2X_4^{2-} \rightarrow X^- + UO_2X_3^-$ Reactions

	B3LYP[a]				CCSD(T)[b]			
X	F	Cl	Br	I	F	Cl	Br	I
E_a	33.0	19.3	16.7	14.0	37.0	24.3	22.2	20.5
ΔE	−19.7	−29.8	−30.9	−31.4	−16.2	−24.4	−24.9	−24.4
ΔG	−27.8	−37.6	−38.7	−39.1	−24.3	−32.2	−32.7	−32.1

[a]Zero-point energy (ZPE) corrections are included in the energies. [b]Single-point CCSD(T) energy calculations at the B3LYP-optimized geometries with inclusion of ZPE corrections and thermal free energy corrections from B3LYP calculation.

dx.doi.org/10.1021/ic4006482 | Inorg. Chem. 2013, 52, 6617−6626

complexes are thermodynamically unstable against dissociation to $UO_2X_3^-$ + X^- with decreasing dynamic stability from X = F to I. The competition between the U−X bonding and the Coulomb repulsions determines the kinetic stabilities of gaseous $UO_2X_4^{2-}$.

■ ASSOCIATED CONTENT

Supporting Information

Complete ref 67 and calculated VDEs of $UO_2X_3^-$ (X = F, Cl, Br, I) from the SO-DFT/PBE and CASSCF/CR-EOM-CCSD(T)/SO methods. This material is available free of charge via the Internet at http://pubs.acs.org.

■ AUTHOR INFORMATION

Corresponding Author

*E-mail: lai-sheng_wang@brown.edu (L.S.W.); junli@mail.tsinghua.edu.cn (J.L.).

Notes

The authors declare no competing financial interest.

■ ACKNOWLEDGMENTS

This work was supported by the U.S. Department of Energy, Office of Basics Energy Sciences, under Grant No. DE-FG02-11ER16261. P.D.D. would like to thank the Nahigian Gift to the Department of Chemistry at Brown University for partial support for this work. Theoretical work was supported by NSFC (20933003, 11079006, 91026003) to J.L. and NSFC (21201106) and the China Postdoctoral Science Foundation (2012M520297) to J.S. Calculations were performed at the Supercomputer Center of the Computer Network Information Center, Chinese Academy of Sciences, Tsinghua National Laboratory for Information Science and Technology, and Shanghai Supercomputing Center. A portion of the calculations was performed using EMSL, a national scientific user facility sponsored by the U.S. Department of Energy's Office of Biological and Environmental Research and located at the Pacific Northwest National Laboratory.

■ REFERENCES

(1) Morss, L. R.; Edelstein, N. M.; Fuger, J. *The Chemistry of the Actinide and Transactinide Elements*, Springer: Dordrecht, The Netherlands, 2006; Vols. *1* and *2*.

(2) Minasian, S. G.; Kieth, J. M.; Batista, E. R.; Boland, K. S.; Christensen, C. N.; Clark, D. L.; Conradson, S. D.; Kozimor, S. A.; Martin, R. L.; Schwarz, D. E.; Shuh, D. K.; Wagner, G. L.; Wilkerson, M. P.; Wolfsberg, L. E.; Yang, P. *J. Am. Chem. Soc.* **2012**, *134*, 5586−5597.

(3) Kozimor, S. A.; Yang, P.; Batista, E. R.; Boland, K. S.; Burns, C. J.; Clark, D. L.; Conradson, S. D.; Martin, R. L.; Wilkerson, M. P.; Wolfsberg, L. E. *J. Am. Chem. Soc.* **2009**, *131*, 12125−12136.

(4) Minasian, S. G.; Boland, K. S.; Feller, R. K.; Gaunt, A. J.; Kozimor, S. A.; May, I.; Reilly, S. D.; Scott, B. L.; Shuh, D. K *Inorg. Chem.* **2012**, *51*, 5728−5736.

(5) Pyykkö, P.; Lohr, L. L. *Inorg. Chem.* **1981**, *20*, 1950−1959.

(6) Kaltsoyannis, N.; Bursten, B. E. *Inorg. Chem.* **1995**, *34*, 2135−2144.

(7) Pepper, M.; Bursten, B. E. *Chem. Rev.* **1991**, *91*, 719−741.

(8) Kovácsa, A.; Konings, R. J. M. *J. Mol. Struct. (THEOCHEM)* **2004**, *684*, 35−42.

(9) Denning, R. G. *Struct. Bonding (Berlin)* **1992**, *79*, 215−276.

(10) Thibaut, E.; Boutique, J.-P.; Verbist, J. J.; Levet, J.-C.; Noelt, H. *J. Am. Chem. Soc.* **1982**, *104*, 5266−5273.

(11) Zhurov, V. V.; Zhurova, E. A.; Stash, A. I.; Pinkerton, A. A. *J. Phys. Chem. A* **2011**, *115*, 13016−13023.

(12) Zhurov, V. V.; Zhurova, E. A.; Pinkerton, A. A. *Inorg. Chem.* **2011**, *50*, 6330−6333.

(13) Groenewold, G. S.; van Stipdonk, M. J.; Oomens, J.; de Jong, W. A.; Gresham, G. L.; McIlwain, M. E. *Int. J. Mass Spectrom.* **2010**, *297*, 67−75.

(14) Seaman, L. A.; Wu, G.; Edelstein, N.; Lukens, W. W.; Magnani, N.; Hayton, T. W. *J. Am. Chem. Soc.* **2012**, *134*, 4931−4940.

(15) Vallet, V.; Wahlgren, U.; Grenthe, I. *J. Phys. Chem. A* **2012**, *116*, 12373−12380.

(16) Wilkerson, M. P.; Burns, C. J.; Paine, R. T.; Scott, B. L. *Inorg. Chem.* **1999**, *38*, 4156−4158.

(17) Berthet, J.-C.; Siffredi, G.; Thuéry, P.; Ephritikhine, M. *Dalton Trans.* **2009**, 3478−3494.

(18) Su, J.; Zhang, K.; Schwarz, W. H. E.; Li, J. *Inorg. Chem.* **2011**, *50*, 2082−2093.

(19) Chakravorti, M. C.; Bandyopadhyay, N. *J. Inorg. Nucl. Chem.* **1971**, *33*, 2565−2571.

(20) Mak, T. C. W.; Yip, W.-H. *Inorg. Chim. Acta* **1985**, *109*, 131−133.

(21) Bühl, M. *Can. J. Chem.* **2009**, *87*, 818−823.

(22) Flint, C. D.; Tanner, P. A. *Mol. Phys.* **1981**, *43*, 933−944.

(23) Denning, R. G.; Snellgrove, T. R.; Woodwark, D. R. *Mol. Phys.* **1976**, *32*, 419−442.

(24) Flint, C. D.; Tanner, P. A. *J. Chem. Soc., Faraday Trans. II* **1978**, *74*, 2210−2217.

(25) Wilson, R. E.; Skanthakumar, S.; Cahill, C. L.; Soderholm, L. *Inorg. Chem.* **2011**, *50*, 10748−10754.

(26) Crawford, M.-J.; Mayer, P. *Inorg. Chem.* **2005**, *44*, 5547−5549.

(27) Chaudhuri, M. K.; Khathing, D. T.; Srinivas, P. *J. Fluorine Chem.* **1992**, *56*, 305−307.

(28) Chaudhuri, M. K.; Srinivas, P. *Polyhedron* **1993**, *12*, 227−234.

(29) Atoji, M.; Mcdermott, M. J. *Acta Crystallogr.* **1970**, *B26*, 1540−1544.

(30) Straka, M.; Dyall, K. G.; Pyykkö, P. *Theor. Chem. Acc.* **2001**, *106*, 393−403.

(31) Vallet, V.; Wahlgren, U.; Schimmelpfennig, B.; Moll, H.; Szabo, Z.; Grenthe, I. *Inorg. Chem.* **2001**, *40*, 3516−3525.

(32) Hennig, C.; Servaes, K.; Nockemann, P.; Hecke, K. V.; Meervelt, L. V.; Wouters, J.; Fluyt, L.; Görller-Walrand, C.; Deun, R. V. *Inorg. Chem.* **2008**, *47*, 2987−2993.

(33) Sornein, M. O.; Mendes, M.; Cannes, C.; Le Naour, C.; Nockemann, P.; Van Hecke, K.; Van Meervelt, L.; Berthet, J. C.; Hennig, C. *Polyhedron* **2009**, *28*, 1281−1286.

(34) Kemp, R. S. *Sci. Global Secur.* **2008**, *16*, 115−125.

(35) Jin, J.; Gondalia, R.; Heaven, M. C. *J. Phys. Chem. A* **2009**, *113*, 12724−12728.

(36) Souter, P. F.; Andrews, L. *J. Mol. Struct.* **1997**, *412*, 161−167.

(37) Dau, P. D.; Su, J.; Liu, H. T.; Liu, J. B.; Huang, D. L.; Li, J.; Wang, L. S. *Chem. Sci.* **2012**, *3*, 1137−1146.

(38) Dau, P. D.; Su, J.; Liu, H. T.; Huang, D. L.; Li, J.; Wang, L. S. *J. Chem. Phys.* **2012**, *137*, 064315.

(39) Denning, R. G. *J. Phys. Chem. A* **2007**, *111*, 4125−4143.

(40) Su, J.; Wang, Y.-L.; Wei, F.; Schwarz, W. H. E.; Li, J. *J. Chem. Theory Comput.* **2011**, *7*, 3293−3303.

(41) Wang, L. S.; Ding, C. F.; Wang, X. B.; Barlow, S. E. *Rev. Sci. Instrum.* **1999**, *70*, 1957−1966.

(42) (a) Wang, X. B.; Wang, L. S. *Rev. Sci. Instrum.* **2008**, *79*, 073108. (b) Dau, P. D.; Liu, H. T.; Huang, D. L.; Wang, L. S. *J. Chem. Phys.* **2012**, *137*, 116101.

(43) Ning, C. G.; Xiong, X. G.; Wang, Y. L.; Li, J.; Wang, L. S. *Phys. Chem. Chem. Phys.* **2012**, *14*, 9323−9329.

(44) Liu, H. T.; Wang, Y. L.; Xiong, X. G.; Dau, P. D.; Piazza, Z.; Huang, D. L.; Xu, C. Q.; Li, J.; Wang, L. S. *Chem. Sci.* **2012**, *3*, 3286−3295.

(45) Perdew, J. P.; Burke, K.; Ernzerhof, M. *Phys. Rev. Lett.* **1996**, *77*, 3865−3868.

(46) ADF 2010.01, http://www.scm.com.

(47) Fonseca Guerra, C. F.; Snijders, J. G.; te Velde, G.; Baerends, E. J. *Theor. Chem. Acc.* **1998**, *99*, 391−403.

(48) Velde, G. T.; Bickelhaupt, F. M.; Baerends, E. J.; Guerra, C. F.; van Gisbergen, S. J. A.; Snijders, J. G.; Ziegler, T. *J. Comput. Chem.* **2001**, *22*, 931−967.
(49) van Lenthe, E.; Baerends, E. J. *J. Comput. Chem.* **2003**, *24*, 1142−1156.
(50) van lenthe, E.; Baerends, E. J.; Snijders, J. G. *J. Chem. Phys.* **1993**, *99*, 4597−4610.
(51) Werner, H. J.; Knowles, P. J.; Lindh, R.; Manby, F. R.; Schütz, M.; et al. *MOLPRO, version 2008.1, a package of ab initio programs*, see http://www.molpro.net.
(52) Wang, X. B.; Wang, Y. L.; Yang, J.; Xing, X. P.; Li, J.; Wang, L. S. *J. Am. Chem. Soc.* **2009**, *131*, 16368−16370.
(53) Wang, Y. L.; Zhai, H. J.; Xu, L.; Li, J.; Wang, L. S. *J. Phys. Chem. A* **2010**, *114*, 1247−1254.
(54) Wang, Y. L.; Wang, X.-B.; Xing, X. P.; Wei, F.; Li, J.; Wang, L. S. *J. Phys. Chem. A* **2010**, *114*, 11244−11251.
(55) Liu, H. T.; Xiong, X. G.; Dau, P. D.; Wang, Y. L.; Li, J.; Wang, L. S. *Chem. Sci.* **2011**, *2*, 2101−2108.
(56) Kowalski, K.; Piecuch, P. *J. Chem. Phys.* **2004**, *120*, 1715−1738.
(57) Valiev, M.; Bylaska, E. J.; Govind, N.; Kowalski, K.; Straatsma, T. P.; Van Dam, H. J. J.; Wang, D.; Nieplocha, J.; Apra, E.; Windus, T. L.; de Jong, W. *Comput. Phys. Commun.* **2010**, *181*, 1477−1489.
(58) http://www.theochem.uni-stuttgart.de/pseudopotential.
(59) Cao, X.; Dolg, M.; Stoll, H. *J. Chem. Phys.* **2003**, *118*, 487−496.
(60) Cao, X.; Dolg, M. *J. Molec. Struct. (THEOCHEM)* **2004**, *673*, 203−209.
(61) Kendall, R. A.; Dunning, T. H.; Harrison, R. J. *J. Chem. Phys.* **1992**, *96*, 6796−6806.
(62) Woon, D. E.; Dunning, T. H. *J. Chem. Phys.* **1993**, *98*, 1358−1371.
(63) Peterson, K. A.; Figgen, D.; Goll, E.; Stoll, H.; Dolg, M. *J. Chem. Phys.* **2003**, *119*, 11113−11123.
(64) Peterson, K. A.; Shepler, B. C.; Figgen, D.; Stoll, H. *J. Phys. Chem. A* **2006**, *110*, 13877−13883.
(65) Becke, A. D. *Phys. Rev. A* **1988**, *38*, 3098−3100.
(66) Lee, C.; Yang, W.; Parr, R. G. *Phys. Rev. B* **1988**, *37*, 785−789.
(67) Frisch, M. J.; et al. *Gaussian 09*, revision B.01; Gaussian, Inc.: Wallingford, CT, 2010.
(68) Weinhold, F.; Landis, C. R. *Valency and Bonding. A Natural Bond Orbital Donor-Acceptor Perspective*; Cambridge University Press: Cambridge, U. K., 2005.
(69) Glendening, E. D.; Badenhoop, J. K.; Reed, A. E.; Carpenter, J. E.; Bohmann, J. A.; Morales, C. M.; Weinhold, F. *NBO 5.0G*; Theoretical Chemistry Institute, University of Wisconsin: Madison, WI, 2004; http://www.chem.wisc.edu/~nbo5.
(70) Ziegler, T.; Rauk, A. *Theor. Chim. Acta* **1977**, *46*, 1.
(71) Bickelhaupt, F. M.; Baerends, E. J. In *Reviews in Computational. Chemistry.*; Lipkowitz, K. B., Boyd, D. B., Eds.; Wiley-VCH: New York, 2000; Vol. *15*, 1−86.
(72) von Hopffgarten, M.; Frenking, G. *WIREs Comput. Mol. Sci.* **2012**, *2*, 43−62.
(73) Dau, P. D.; Su, J.; Liu, H. T.; Huang, D. L.; Wei, F.; Li, J.; Wang, L. S. *J. Chem. Phys.* **2012**, *136*, 194304.
(74) van Lenthe, E.; Snijders, J. G.; Baerends, E. J. *J. Chem. Phys.* **1996**, *105*, 6505−6516.
(75) Griffiths, D J. *Introduction to Quantum Mechanics*, 2nd ed.; Prentice Hall: New Jersey, 2004.
(76) Case, D. A.; Yang, C. Y. *J. Chem. Phys.* **1980**, *72*, 3443−3448.
(77) Xiao, H.; Hu, H.-S.; Schwarz, W. H. E.; Li, J. *J. Phys. Chem. A* **2010**, *114*, 8837−8844.
(78) Gutsev, G. L.; Boldyrev, A. I. *Chem. Phys. Lett.* **1981**, *56*, 277−283.
(79) Yang, X.; Waters, T.; Wang, X. B.; O'Hair, R. A. J.; Wedd, A. G.; Li, J.; Dixon, D. A.; Wang, L. S. *J. Phys. Chem. A* **2004**, *108*, 10089−10093.
(80) Michalak, A.; DeKock, R. L.; Ziegler, T. *J. Phys. Chem. A* **2008**, *112*, 7256−7263.
(81) Glendening, E. D.; Weinhold, F. *J. Comput. Chem.* **1998**, *19*, 593−609.
(82) Glendening, E. D.; Weinhold, F. *J. Comput. Chem.* **1998**, *19*, 610−627.
(83) Glendening, E. D.; Badenhoop, J. K.; Weinhold, F. *J. Comput. Chem.* **1998**, *19*, 628−646.
(84) Reed, A. E.; Curtiss, L. A.; Weinhold, F. *Chem. Rev.* **1988**, *88*, 899−926.
(85) Aquino, F.; Govind, N.; Autschbach, J. *J. Chem. Theory Comput.* **2010**, *6*, 2669−2686.
(86) Wang, X. B.; Wang, L. S. *Nature* **1999**, *400*, 245−248.
(87) Wang, L. S.; Wang, X. B. *J. Phys. Chem. A* **2000**, *104*, 1978−1990.
(88) Wang, L. S.; Ding, C. F.; Wang, X. B.; Nicholas, J. B. *Phys. Rev. Lett.* **1998**, *81*, 2667−2670.